Effect of the irreversible A+B → C reaction on the onset and the growth of the buoyancy-driven instability in a porous medium: Asymptotic, linear, and nonlinear stability analyses

Min Chan Kim*
Department of Chemical Engineering, Jeju National University, Jeju 63243, Republic of Korea

(Received 10 March 2019; published 2 July 2019)

Taking different diffusivities into account, the effect of irreversible A+B →C reaction on the growth of a buoyancy-driven instability in a Hele-Shaw cell is analyzed theoretically. For the limiting cases of infinitely fast reaction, an asymptotic stability analysis is conducted based on base density profile. To confirm the asymptotic stability analysis, under the linear stability theory, new linear stability equations are derived and solved numerically. In addition, fully nonlinear numerical simulations are conducted using the Fourier spectral method. The present asymptotic and linear stability analyses and nonlinear numerical simulations are in good agreement, and they modify the previous general classification of stability. For some cases where a stable barrier is sandwiched by two unstable regions, we also conducted linear and nonlinear analyses. It is interesting that for a certain case, instabilities with different wavelengths are possible below and above a central stable barrier.

DOI: 10.1103/PhysRevFluids.4.073901

I. INTRODUCTION

The gravitational instability in a fluid layer is a well-known phenomenon and has a long history. Lord Rayleigh [1] proved that the fluid layer is gravitationally unstable if the heavier fluid locates over the lighter one. Later, Taylor [2] examined the stability properties of fictitious horizontal interfaces between two immiscible fluids in a homogeneous isotropic porous medium. Under these historical backgrounds, this buoyancy-driven motion is referred to as Rayleigh-Taylor instability or gravitational fingering. Later, considering the broadening of the interface due to the diffusion, Wooding [3] analyzed the onset of fingering in a miscible fluids saturated porous medium. This kind of instability in a nonreactive miscible solution occurs in many engineering applications, such as pollutant transport in groundwater and geological storage of greenhouse gas.

In reactive systems, chemical reactions can accelerate or impede the instability motion under the gravity field [4–7]. The instability motion in reactive systems might be encountered in many engineering applications in porous media such as *in situ* oil recovery, *in situ* groundwater remediation and a CO_2 sequestration process [8]. Recently, Almarcha *et al.* [9,10] and Kuster *et al.* [11] experimentally analyzed the effect of gravity on the stability of a reactive interface in a Hele-Shaw cell. In their experiments, they employed acid-base reactions which can be treated by an infinitely fast reaction. Later, Lemaigre *et al.* [12] studied experimentally and numerically the onset and growth of the asymmetric Rayleigh-Taylor and double-diffusive fingers in the acid-base reaction system confined in a Hele-Shaw cell. Theoretically, Hejazi and Azaiez [13,14] considered the effects of viscosity variation and transverse flow on the instabilities of a reactive front. However,

*mckim@cheju.ac.kr

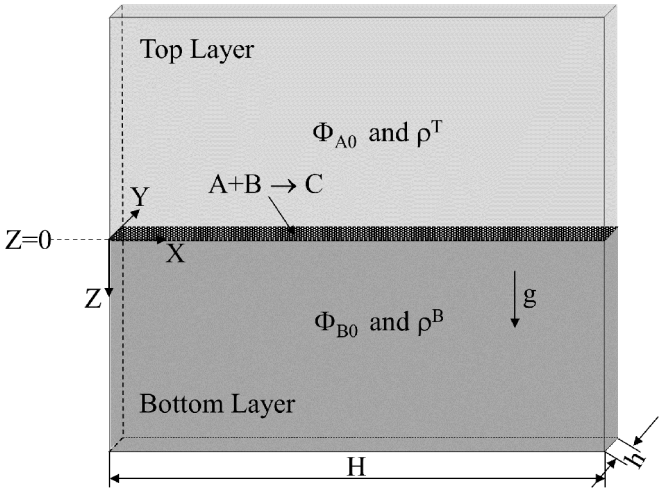

FIG. 1. Schematic diagram of the system considered here.

their linear stability analysis strongly depends on the conventional quasi-steady state approximation in the global (τ, z)- domain (here we call their method QSSAz). As discussed by Trevelyan *et al.* [15], the conventional QSSAz cannot predict the stability characteristics accurately, especially for the initial stage. Kim [16] analyzed theoretically and numerically the effect of the irreversible second-order A+B →C reaction on the growth of a buoyancy-driven instability by neglecting the effect of the different diffusivities and reactants ratio. Recently, by considering the different diffusivities and reactants ratio, Trevelyan *et al.* [17] suggested a general classification on the density profile. However, they did not try to verify their classification through systematic stability analyses. Therefore, systematic analyses are strongly needed to understand a chemical reaction and different diffusivities effects on the buoyancy-driven instability.

In the present study, we focused on the effects of an irreversible A+B →C reaction on the onset and the growth of the buoyancy-driven instabilities. Because we did not require that all chemical components have the same diffusivity, the present study explains the physicochemical phenomena more rigorously. For the infinitely fast reaction, we derived asymptotic concentration and density profiles and classified asymptotic stability regimes based on the density profile. For some typical cases, we conducted linear stability analyses and nonlinear numerical simulations to prove the validity of the present asymptotic stability results. We also conducted the linear and nonlinear analyses for interesting cases where a stable region is sandwiched between unstable regions. For the various cases, the present asymptotic, linear, and nonlinear stability results were in good agreement.

II. GOVERNING EQUATIONS AND BASE FIELDS

The system considered here is a Hele-Shaw cell schematized in Fig. 1. Inside a Hele-Shaw cell, a solution of a reactant A at concentration C_{A0} is placed on top of a solution containing a reactant B at concentration C_{B0}. A chemical reaction occurs between the two chemical species A and B and a product C is produced in the following irreversible bimolecular elementary reaction:

$$A + B \rightarrow C. \tag{1}$$

If the density of product C is different from that of either reactant, the flow system can be hydrodynamically unstable and induce the density-driven convective motion.

The governing equations are those for the conservation of mass, the conservation of momentum in the form of Darcy's law and the convection-dispersion-reaction mass balance equation [18]

$$\nabla \cdot \mathbf{U} = 0, \tag{2}$$

$$\nabla P = -\frac{\mu}{K}\mathbf{U} + \rho \mathbf{g}, \tag{3}$$

$$\frac{\partial \Phi_i}{\partial t} + \mathbf{U} \cdot \nabla \Phi_i = D_i \nabla^2 \Phi_i + n_i k_r \Phi_\mathrm{A} \Phi_\mathrm{B}, \tag{4}$$

where $i = \mathrm{A}, \mathrm{B}, \text{and } \mathrm{C}$, and $-n_\mathrm{A} = -n_\mathrm{B} = n_\mathrm{C} = 1$. Here, $\mathbf{U}$ is the velocity vector, P the pressure, μ the dynamic viscosity, K the permeability, ρ the density, $\mathbf{g}$ the gravitational acceleration vector, Φ_i the concentration of chemical species i, t the time, D_i the diffusion coefficient chemical species i, and k_r the reaction constant of the reaction (1). The solution density is assumed to depend linearly on the concentrations as [18]

$$\rho = \rho_r \left(1 + \sum\nolimits_i \alpha_i \Phi_i\right), \tag{5}$$

where ρ_r is the density of the solvent, and $\alpha_i (= \rho_r^{-1} \partial \rho / \partial \Phi_i)$ is the concentration expansion coefficient of species i. The proper initial and boundary conditions are

$$\mathbf{U} = \mathbf{0}, \quad \Phi_\mathrm{A} = \begin{cases} \Phi_{\mathrm{A},0} & Z < 0 \\ 0 & Z > 0 \end{cases}, \quad \Phi_\mathrm{B} = \begin{cases} 0 & Z < 0 \\ \Phi_{\mathrm{B},0} & Z > 0 \end{cases} \quad \text{and} \quad \Phi_\mathrm{C} = 0 \text{ at } t = 0, \tag{6a}$$

$$\mathbf{U} \to \mathbf{0}, \quad \Phi_\mathrm{A} \to \Phi_{\mathrm{A},0}, \quad \Phi_\mathrm{B} \to 0 \quad \text{and} \quad \Phi_\mathrm{C} \to 0 \quad \text{as } Z \to \infty, , \tag{6b}$$

$$\mathbf{U} \to \mathbf{0}, \quad \Phi_\mathrm{A} \to 0, \quad \Phi_\mathrm{B} \to \Phi_{\mathrm{B},0} \quad \text{and} \quad \Phi_\mathrm{C} \to 0 \quad \text{as } Z \to \infty. \tag{6c}$$

The above governing equation can be written in dimensionless form:

$$\nabla \cdot \mathbf{u} = 0, \tag{7}$$

$$\mathbf{u} = -\nabla p + \mathbf{k}\bar{\rho}, \tag{8}$$

$$\frac{\partial \phi_i}{\partial \tau} + \mathbf{u} \cdot \nabla \phi_i = \delta_i \nabla^2 \phi_i + n_i \mathrm{Da} \phi_\mathrm{A} \phi_\mathrm{B}, \tag{9}$$

using the following relations:

$$\mathbf{X} = l\mathbf{x}, \quad t = \frac{l^2}{D_\mathrm{A}}\tau, \quad \mathbf{U} = \frac{D_\mathrm{A}}{l}\mathbf{u}, \quad P = \frac{D_\mathrm{A}\mu}{K}p + \frac{D_\mathrm{A}\mu}{K\alpha_\mathrm{A}\Phi_{\mathrm{A}0}}z, \quad \Phi_i = \Phi_{\mathrm{A}0}\phi_i \quad \text{and} \quad D_i = D_\mathrm{A}\delta_i, \tag{10}$$

where $l\{=D_\mathrm{A}\nu/(|\mathbf{g}|\alpha_\mathrm{A}\Phi_{\mathrm{A}0}K)\}$ is chosen as the length scale. In addition, $\mathbf{k}$ is the unit vector parallel to $\mathbf{g}$, i.e., z axis is increasing in the downwards direction, and $\nu (= \mu/\rho_r)$ is the kinematic viscosity. The dimensionless density $\bar{\rho}$ can be expressed as

$$\bar{\rho}\left(= \frac{\rho - \rho_r}{\rho_r \alpha_\mathrm{A} \Phi_{\mathrm{A}0}}\right) = \sum_i \beta_i \phi_i, \tag{11}$$

where $\beta_i = \alpha_i/\alpha_\mathrm{A}$. The Damköhler Da, which represents the ratio of hydrodynamic to chemical characteristic times, is defined as

$$\mathrm{Da} = \frac{k_r \Phi_{\mathrm{A}0} l^2}{D_\mathrm{A}}. \tag{12}$$

By expanding $\mathbf{u}(\tau, x, z) = \mathbf{0} + \mathbf{u}_1(\tau, x, z)$ and $\phi_i(\tau, x, z) = \phi_{i,0}(\tau, z) + \phi_{i,1}(\tau, x, z)$, the base-state concentrations $\phi_{i,0}(\tau, z)$ can be obtained by solving the following reaction-diffusion equation:

$$\frac{\partial \phi_{i,0}}{\partial \tau} = \delta_i \frac{\partial^2 \phi_{i,0}}{\partial z^2} + n_i \mathrm{Da} \phi_{\mathrm{A},0} \phi_{\mathrm{B},0}, \tag{13}$$

The proper initial and boundary conditions are

$$\phi_{\mathrm{A},0}(0, z) = H(-z), \quad \phi_{\mathrm{B},0}(0, z) = r_{\mathrm{B}} H(z) \quad \text{and} \quad \phi_{\mathrm{C},0}(0, z) = 0, \tag{14a}$$

$$\phi_{\mathrm{A},0}(\tau, z) \to 1, \quad \phi_{\mathrm{B},0}(\tau, z) \to 0 \quad \text{and} \quad \phi_{\mathrm{C},0}(\tau, z) \to 0 \quad \text{as} \, z \to -\infty, \tag{14b}$$

$$\phi_{\mathrm{A},0}(\tau, z) \to 0, \quad \phi_{\mathrm{B},0}(\tau, z) \to r_{\mathrm{B}} \quad \text{and} \quad \phi_{\mathrm{C},0}(\tau, z) \to 0 \quad \text{as} \, z \to \infty, \tag{14c}$$

where $H(z)$ is the Heaviside step function and $r_{\mathrm{B}} = \Phi_{\mathrm{B}0}/\Phi_{\mathrm{A}0}$. In an instantaneous chemical reaction, such as acid-base reaction, there exists a reaction front above or below which one of reactants cannot exist. For this limiting case, the above reaction-diffusion equations can be rewritten as

$$\frac{\partial \phi_{i,0}}{\partial \tau} = \delta_i \nabla^2 \phi_{i,0}, \tag{15}$$

under the condition of $\phi_{\mathrm{A},0}(\tau, z \geqslant z_f) = 0$ and $\phi_{\mathrm{B},0}(\tau, z \leqslant z_f) = 0$. Here, z_f means the position where the instantaneous reaction proceeds. The above concentration fields should satisfy the following mass balances:

$$\left(\sum_{j, j \neq \mathrm{B}} \phi_{j,0} \right)^{\mathrm{T}} = \left(\sum_{j, j \neq \mathrm{B}} \phi_{j,0} \right)^{\mathrm{B}} \tag{16a}$$

and

$$\left(\sum_{k, k \neq \mathrm{A}} \phi_{k,0} \right)^{\mathrm{T}} = \left(\sum_{k, k \neq \mathrm{A}} \phi_{k,0} \right)^{\mathrm{B}} \quad \text{at} \quad z = z_f, \tag{16b}$$

$$\left(\sum_{j, j \neq \mathrm{B}} \delta_j \frac{\partial \phi_{j,0}}{\partial z} \right)^{\mathrm{T}} = \left(\sum_{j, j \neq \mathrm{B}} \delta_j \frac{\partial \phi_{j,0}}{\partial z} \right)^{\mathrm{B}} \tag{17a}$$

and

$$\left(\sum_{k, k \neq \mathrm{A}} \delta_k \frac{\partial \phi_{k,0}}{\partial z} \right)^{\mathrm{T}} = \left(\sum_{k, k \neq \mathrm{A}} \delta_k \frac{\partial \phi_{k,0}}{\partial z} \right)^{\mathrm{B}} \quad \text{at} \quad z = z_f. \tag{17b}$$

where the superscripts 'T' and 'B' mean the top and bottom layers, respectively. Equations (16a) and (16b) represent the continuities of the concentrations of (A+C) and (B+C), respectively. Equations (17a) and (17b) correspond to the flux continuities for (A+C) and (B+C), respectively.

By considering the above findings, in the large Damköhler number limit or in the large time limit, the base-state solutions can be obtained analytically as

$$(\phi_{\mathrm{A},0}, \phi_{\mathrm{B},0}, \phi_{\mathrm{C},0})^T = \left\{ 1 - \frac{\mathrm{erfc}(-\zeta/2)}{\mathrm{erfc}(-\zeta_f/2)}, 0, r_{\mathrm{C}} \frac{\mathrm{erfc}(-\zeta/\sqrt{4\delta_{\mathrm{C}}})}{\mathrm{erfc}(-\zeta_f/\sqrt{4\delta_{\mathrm{C}}})} \right\} \quad \text{for} \, \zeta < \zeta_f, \tag{18a}$$

$$(\phi_{\mathrm{A},0}, \phi_{\mathrm{B},0}, \phi_{\mathrm{C},0})^{\mathrm{B}} = \left\{ 0, r_{\mathrm{B}} - r_{\mathrm{B}} \frac{\mathrm{erfc}(\zeta/\sqrt{4\delta_{\mathrm{B}}})}{\mathrm{erfc}(\zeta_f/\sqrt{4\delta_{\mathrm{B}}})}, r_{\mathrm{C}} \frac{\mathrm{erfc}(\zeta/\sqrt{4\delta_{\mathrm{C}}})}{\mathrm{erfc}(\zeta_f/\sqrt{4\delta_{\mathrm{C}}})} \right\} \quad \text{for} \, \zeta > \zeta_f, \tag{18b}$$

where $\zeta = z/\sqrt{\tau}$ and $\zeta_f = z_f/\sqrt{\tau}$. Here, undetermined constants, ζ_f and r_C can be determined as

$$\mathrm{erfc}(\zeta_f/\sqrt{4\delta_B})\exp\left\{\frac{\zeta_f^2}{4}\left(\frac{1}{\delta_B}-1\right)\right\} = r_B\sqrt{\delta_B}\mathrm{erfc}(-\zeta_f/2), \tag{19}$$

$$r_C = \frac{\mathrm{erfc}(\zeta_f/\sqrt{4\delta_C})\mathrm{erfc}(-\zeta_f/\sqrt{4\delta_C})}{2\sqrt{\delta_C}\mathrm{erfc}(-\zeta_f/2)}\exp\left\{\frac{\zeta_f^2}{4}\left(\frac{1}{\delta_C}-1\right)\right\}, \tag{20}$$

by considering the mass flux balances Eq. (17).

III. ASYMPTOTIC STABILITY ANALYSIS OR GENERAL CLASSIFICATION

Using Eq. (11) and the above relations, the following dimensionless densities can be derived:

$$\bar{\rho}_0^T = 1 - \frac{\mathrm{erfc}(-\zeta/2)}{\mathrm{erfc}(-\zeta_f/2)} + \beta_C r_C \frac{\mathrm{erfc}(-\zeta/\sqrt{4\delta_C})}{\mathrm{erfc}(-\zeta_f/\sqrt{4\delta_C})}, \tag{21a}$$

$$\bar{\rho}_0^B = r_B\beta_B\left\{1 - \frac{\mathrm{erfc}(\zeta/\sqrt{4\delta_B})}{\mathrm{erfc}(\zeta_f/\sqrt{4\delta_B})}\right\} + r_C\beta_C\frac{\mathrm{erfc}(\zeta/\sqrt{4\delta_C})}{\mathrm{erfc}(\zeta_f/\sqrt{4\delta_C})}. \tag{21b}$$

According to Trevelyan *et al.* [17], there are a total of 62 different types of density profiles. It is well-known that even a gravitationally stable density profile can induce an instability due to differential diffusive effects, and the stability regime can be identified from the asymptotic density profile.

Using the above density functions, we can get the following density-gradient related quantities:

$$\frac{\partial\bar{\rho}_0^T}{\partial\zeta} = -\frac{1}{\mathrm{erfc}(-\zeta_f/2)\sqrt{\pi}}\exp\left(-\frac{\zeta^2}{4}\right) + \frac{r_C\beta_C}{\mathrm{erfc}(-\zeta_f/\sqrt{4\delta_C})\sqrt{\pi\delta_C}}\exp\left(-\frac{\zeta^2}{4\delta_C}\right), \tag{22a}$$

$$\frac{\partial\bar{\rho}_0^B}{\partial\zeta} = \frac{r_B\beta_B}{\mathrm{erfc}(\zeta_f/\sqrt{4\delta_B})\sqrt{\pi\delta_B}}\exp\left(-\frac{\zeta^2}{4\delta_B}\right) - \frac{r_C\beta_C}{\mathrm{erfc}(\zeta_f/\sqrt{4\delta_C})\sqrt{\pi\delta_C}}\exp\left(-\frac{\zeta^2}{4\delta_C}\right), \tag{22b}$$

$$\frac{1}{\zeta}\frac{\partial^2\bar{\rho}_0^T}{\partial\zeta^2} = \frac{1}{2\mathrm{erfc}(-\zeta_f/2)\sqrt{\pi}}\exp\left(-\frac{\zeta^2}{4}\right) - \frac{r_C\beta_C}{2\delta_C\mathrm{erfc}(-\zeta_f/\sqrt{4\delta_C})\sqrt{\pi\delta_C}}\exp\left(-\frac{\zeta^2}{4\delta_C}\right), \tag{23a}$$

$$\frac{1}{\zeta}\frac{\partial^2\bar{\rho}_0^B}{\partial\zeta^2} = -\frac{r_B\beta_B}{2\delta_B\mathrm{erfc}(\zeta_f/\sqrt{4\delta_B})\sqrt{\pi\delta_B}}\exp\left(-\frac{\zeta^2}{4\delta_B}\right) + \frac{r_C\beta_C}{2\delta_C\mathrm{erfc}(\zeta_f/\sqrt{4\delta_C})\sqrt{\pi\delta_C}}\exp\left(-\frac{\zeta^2}{4\delta_C}\right), \tag{23b}$$

By setting $\partial\bar{\rho}/\partial\zeta = 0$ and $\zeta^{-1}\partial^2\bar{\rho}/\partial\zeta^2 = 0$, the following density-extremum points, ζ_e, and density-inflection points, ζ_i, can be obtained:

$$\left(\zeta_e^T\right)^2 - \zeta_f^2 = \frac{4\delta_C}{1-\delta_C}\ln\left\{\frac{\beta_C}{2\delta_C}\mathrm{erfc}(\zeta_f/\sqrt{4\delta_C})\right\} \tag{24a}$$

and

$$\left(\zeta_e^B\right)^2 - \zeta_f^2 = \frac{4\delta_B\delta_C}{\delta_B-\delta_C}\ln\left\{\frac{\beta_C\delta_B}{2\beta_B\delta_C}\mathrm{erfc}(-\zeta_f/\sqrt{4\delta_C})\right\}. \tag{24b}$$

$$\left(\zeta_i^T\right)^2 - \zeta_f^2 = \frac{4\delta_C}{1-\delta_C}\ln\left\{\frac{\beta_C}{2\delta_C^2}\mathrm{erfc}(\zeta_f/\sqrt{4\delta_C})\right\} \tag{25a}$$

and

$$\left(\zeta_i^{\mathrm{B}}\right)^2 - \zeta_f^2 = \frac{4\delta_{\mathrm{B}}\delta_{\mathrm{C}}}{\delta_{\mathrm{B}} - \delta_{\mathrm{C}}} \ln\left\{\frac{\beta_{\mathrm{C}}\delta_{\mathrm{B}}^2}{2\beta_{\mathrm{B}}\delta_{\mathrm{C}}^2}\mathrm{erfc}(-\zeta_f/\sqrt{4\delta_{\mathrm{C}}})\right\}. \tag{25b}$$

Trevelyan *et al.*'s [17] classified the Rayleigh-Taylor (RT) instability, the diffusive-layer convection (DLC), and the double diffusive convection (DD) regions. Here, using the above density gradient functions, we systematically classify the asymptotic stability regimes. The system can be globally unstable if the density profile decreases monotonically, $\partial\bar{\rho}/\partial\zeta|_{\zeta=\zeta_f} < 0$ and $\zeta_e^2 < 0$. The condition of $\zeta_e^2 < 0$ means that the density extrema points have imaginary value and therefore, the first derivative of the density profile doesn't change its sign for the whole domain. Furthermore, the system can be locally unstable if the density profile has its extrema, $\partial\bar{\rho}/\partial\zeta|_{\zeta=\zeta_f} < 0$ and $\zeta_e^2 > 0$, or $\partial\bar{\rho}/\partial\zeta|_{\zeta=\zeta_f} > 0$ and $\zeta_e^2 > 0$. The above suggestions mean that the system is stably stratified if the density profile increases monotonically, i.e., $\partial\bar{\rho}/\partial\zeta|_{\zeta=\zeta_f} > 0$ and $\zeta_e^2 < 0$. However, in the double diffusive cases such as the salt-finger system [19], instabilities are possible even for the systems having a monotonically increasing density profile. Here, we focused on the stability of the system that is monotonically increasing.

Trevelyan *et al.*'s [17] analyzed the double-diffusive convection (DD) limit by applying the following conventional relation:

$$\frac{-\beta_{\mathrm{C}}(\partial\phi_{\mathrm{C},0}/\partial\zeta)}{(\partial\phi_{\mathrm{A},0}/\partial\zeta)} < \delta_{\mathrm{C}}, \tag{26}$$

which is adopted from the dynamic stability limit for the salt-finger system [19]. However, as pointed out by Huppert and Manins [19], there are some simplifications and bold assumptions. They derived Eq. (23) by combining the linear stability condition for the bounded domain [0,1] (see Eq. (2) of Huppert and Manins [19]), and the density profiles for the unbounded domain $(-\infty,\infty)$ (see Eq. (7) of Huppert and Manins [19]). However, this stability criterion cannot apply to the ternary systems where cross-diffusion effects cannot be ignored. To overcome this limitation, Costantino *et al.* [20], Vitagliano *et al.* [21], Kim and Song [22], and Kim and Cardoso [23] proposed that this kind of instability is possible if the density profile is monotonically increasing with inflection points. In the present upper layer, we employed the following conditions:

$$\left.\frac{\partial\bar{\rho}_0^{\mathrm{T}}}{\partial\zeta}\right|_{\zeta=\zeta_f} > 0, \quad \left(\zeta_e^{\mathrm{T}}\right)^2 < 0 \quad \text{and} \quad \left(\zeta_i^{\mathrm{T}}\right)^2 > 0 \quad \text{for} \quad \zeta_f > 0, \tag{27a}$$

and

$$\left.\frac{\partial\bar{\rho}_0^{\mathrm{T}}}{\partial\zeta}\right|_{\zeta=\zeta_f} > 0, \quad \left(\zeta_e^{\mathrm{T}}\right)^2 - \zeta_f^2 < 0 \quad \text{and} \quad \left(\zeta_i^{\mathrm{T}}\right)^2 - \zeta_f^2 > 0 \quad \text{for} \quad \zeta_f \leqslant 0, \tag{27b}$$

rather than the conventional one, Eq. (26). The above conditions are equivalent to

$$U_1 < \beta_{\mathrm{C}} < \delta_{\mathrm{C}}U_1 \quad \text{if } \delta_{\mathrm{C}} > 1 \quad \text{and} \quad \zeta_f > 0, \tag{28a}$$

$$U_2 < \beta_{\mathrm{C}} < \delta_{\mathrm{C}}U_2 \quad \text{if } \delta_{\mathrm{C}} > 1 \quad \text{and} \quad \zeta_f \leqslant 0, \tag{28b}$$

where

$$U_1 = U_2 \exp\left\{\frac{\zeta_f^2}{4}\left(1 - \frac{1}{\delta_{\mathrm{C}}}\right)\right\} \tag{29a}$$

and

$$U_2 = \frac{2\delta_{\mathrm{C}}}{\mathrm{erfc}(\zeta_f/\sqrt{4\delta_{\mathrm{C}}})}, \tag{29b}$$

which were already defined by Trevelyan *et al.* [17].

Similarly, DD with density inversion is possible if

$$\left.\frac{\partial \bar{\rho}_0^{\mathrm{T}}}{\partial \zeta}\right|_{\zeta=\zeta_f} > 0 \quad \text{and} \quad 0 < \left(\zeta_e^{\mathrm{T}}\right)^2 < \zeta_f^2 \quad \text{for } \zeta_f > 0, \tag{30}$$

i.e.,

$$U_2 < \beta_{\mathrm{C}} < U_1 \quad \text{if } \delta_{\mathrm{C}} > 1 \quad \text{and} \quad \zeta_f > 0. \tag{31}$$

Based on the above findings, the top layer is unconditionally stable if

$$\beta_{\mathrm{C}} > \delta_{\mathrm{C}} U_1, \quad \zeta_f > 0 \quad \text{and} \quad \delta_{\mathrm{C}} > 1, \tag{32a}$$

$$\beta_{\mathrm{C}} > \delta_{\mathrm{C}} U_2, \quad \zeta_f \leqslant 0 \quad \text{and} \quad \delta_{\mathrm{C}} > 1. \tag{32b}$$

For the case of $\zeta_f > 0$, the above criterion, Eq. (32a) obtained from Eq. (28a), is slightly different from Trevelyan *et al.*'s [17] one, i.e., $\beta_{\mathrm{C}} > \delta_{\mathrm{C}} U_2$ and $\delta_{\mathrm{C}} > 1$, which is derived from Eq. (26).

If we apply the above procedure to the bottom layer, then we can obtain the stability criteria:

$$\frac{1}{L_2} < \frac{\beta_{\mathrm{B}}}{\beta_{\mathrm{C}}} < \frac{1}{L_2}\frac{\delta_{\mathrm{B}}}{\delta_{\mathrm{C}}} \quad \text{if } \delta_{\mathrm{B}} > \delta_{\mathrm{C}} \quad \text{and} \quad \zeta_f \geqslant 0, \tag{33a}$$

$$\frac{1}{L_1} < \frac{\beta_{\mathrm{B}}}{\beta_{\mathrm{C}}} < \frac{1}{L_1}\frac{\delta_{\mathrm{B}}}{\delta_{\mathrm{C}}} \quad \text{if } \delta_{\mathrm{B}} > \delta_{\mathrm{C}} \quad \text{and} \quad \zeta_f < 0. \tag{33b}$$

for the double diffusive instability without density inversion, and

$$\frac{1}{L_2} < \frac{\beta_{\mathrm{B}}}{\beta_{\mathrm{C}}} < \frac{1}{L_1} \quad \text{if } \delta_{\mathrm{B}} > \delta_{\mathrm{C}} \quad \text{and} \quad \zeta_f < 0, \tag{34}$$

for the double diffusive instability with density inversion. Here,

$$L_1 = L_2 \exp\left\{\frac{\zeta_f^2}{4}\left(\frac{1}{\delta_{\mathrm{B}}} - \frac{1}{\delta_{\mathrm{C}}}\right)\right\} \quad \text{and} \quad L_2 = \frac{2\delta_{\mathrm{C}}}{\delta_{\mathrm{B}}\mathrm{erfc}(-\zeta_f/\sqrt{4\delta_{\mathrm{C}}})} \tag{35}$$

were already defined by Trevelyan *et al.* [17]. By combining Eqs. (33b) and (34), for the case of $\delta_{\mathrm{B}} > \delta_{\mathrm{C}}$ and $\zeta_f < 0$, double diffusive instability is possible:

$$\frac{1}{L_2} < \frac{\beta_{\mathrm{B}}}{\beta_{\mathrm{C}}} < \frac{1}{L_1} \quad \text{if } \delta_{\mathrm{B}} > \delta_{\mathrm{C}} \quad \text{and} \quad \zeta_f < 0. \tag{36}$$

So, the lower layer is unconditionally stable if

$$\frac{\beta_{\mathrm{B}}}{\beta_{\mathrm{C}}} > \frac{1}{L_2}\frac{\delta_{\mathrm{B}}}{\delta_{\mathrm{C}}}, \quad \delta_{\mathrm{B}} > \delta_{\mathrm{C}} \quad \text{and} \quad \zeta_f \geqslant 0, \tag{37a}$$

$$\frac{\beta_{\mathrm{B}}}{\beta_{\mathrm{C}}} > \frac{1}{L_1}\frac{\delta_{\mathrm{B}}}{\delta_{\mathrm{C}}}, \quad \delta_{\mathrm{B}} > \delta_{\mathrm{C}} \quad \text{and} \quad \zeta_f < 0. \tag{37b}$$

For the case of $\zeta_f < 0$, the present stability limit, $(\beta_{\mathrm{B}}/\beta_{\mathrm{C}}) > L_1^{-1}(\delta_{\mathrm{B}}/\delta_{\mathrm{C}})$, obtained from the existence of the density inflection point, i.e., Eq. (37b), is slightly different from Trevelyan *et al.*'s [17] condition, i.e., $(\beta_{\mathrm{B}}/\beta_{\mathrm{C}}) > L_2^{-1}(\delta_{\mathrm{B}}/\delta_{\mathrm{C}})$ and $\delta_{\mathrm{B}} > \delta_{\mathrm{C}}$, which was derived from $\frac{-\beta_{\mathrm{C}}(\partial\phi_{\mathrm{C},0}/\partial\zeta)}{\beta_{\mathrm{B}}(\partial\phi_{\mathrm{B},0}/\partial\zeta)} < \frac{\delta_{\mathrm{C}}}{\delta_{\mathrm{B}}}$. Since $L_2 > L_1$ for the case of $\delta_{\mathrm{B}} > \delta_{\mathrm{C}}$, the stability of $L_2^{-1}(\delta_{\mathrm{B}}/\delta_{\mathrm{C}}) < (\beta_{\mathrm{B}}/\beta_{\mathrm{C}}) < L_1^{-1}(\delta_{\mathrm{B}}/\delta_{\mathrm{C}})$ should be checked through a thorough stability analysis.

By combining the above findings, Eqs. (32) and (36), the system is unconditionally stable if

$$\delta_{\mathrm{C}} U_1 < \beta_{\mathrm{C}} < \beta_{\mathrm{B}} L_2 \frac{\delta_{\mathrm{C}}}{\delta_{\mathrm{B}}}, \quad \zeta_f > 0 \quad \text{and} \quad \delta_{\mathrm{B}} \geqslant \delta_{\mathrm{C}} \geqslant 1, \tag{38a}$$

$$\delta_{\mathrm{C}} U_2 < \beta_{\mathrm{C}} < \beta_{\mathrm{B}} L_1 \frac{\delta_{\mathrm{C}}}{\delta_{\mathrm{B}}}, \quad \zeta_f < 0 \quad \text{and} \quad \delta_{\mathrm{B}} \geqslant \delta_{\mathrm{C}} \geqslant 1, \tag{38b}$$

which is different from Trevelyan *et al.*'s [17] following condition:

$$\delta_C U_2 < \beta_C < \beta_B L_2 \frac{\delta_C}{\delta_B} \quad \text{and} \quad \delta_B \geqslant \delta_C \geqslant 1. \tag{39}$$

The above stability limit is derived from the Eqs. (32) and (37). For the limiting cases of $\delta_B = \delta_C = 1$ or $\zeta_f = 0$, the above two conditions are identical. Furthermore, for the case of $\delta_B = \delta_C = 1$, the above condition are identical with the following unconditionally stable condition [16]:

$$2 \leqslant \beta_C \leqslant 2\beta_B \quad \text{for} \quad \delta_B = \delta_C = 1. \tag{40}$$

IV. LINEAR STABILITY ANALYSIS

A. Linear stability equations

Under the linear stability theory, the following dimensionless stability equations are obtained by perturbing Eqs. (7)–(9):

$$\nabla^2 w_1 = \nabla_1^2 \Big(\sum\nolimits_i \beta_i \phi_{i,1} \Big), \tag{41}$$

$$\frac{\partial \phi_{i,1}}{\partial \tau} + w_1 \frac{\partial \phi_{i,0}}{\partial z} = \delta_i \nabla^2 \phi_{i,1} + n_i \mathrm{Da} (\phi_{A,0} \phi_{B,1} + \phi_{A,1} \phi_{B,0}), \tag{42}$$

where $\nabla_1^2 = \partial^2/\partial x^2$ and w_1 is the vertical velocity component. The density is decomposed as $\bar{\rho} = \bar{\rho}_0 + \bar{\rho}_1$, $\bar{\rho}_0 = \sum_i \beta_i \phi_{i,0}$, and $\bar{\rho}_1 = \sum_i \beta_i \phi_{i,1}$. The proper boundary conditions are

$$w_1 \to 0 \quad \text{and} \quad \phi_{i,1} \to 0 \quad \text{as } z \to \pm\infty. \tag{43}$$

It is well-known that the disturbances which are localized near the reaction front cannot be accurately captured in the (τ, z)-domain, since the dominant operator, $\partial^2/\partial z^2$, does not have localized eigenfunctions that vanish at the infinite boundaries [24–26]. Following the standard procedure, in the similar (τ, ζ)-domain, we can reformulate Eqs. (41)–(43) as

$$(D^2 - a^{*2}) w_1 = -a^{*2} \Big(\sum\nolimits_i \beta_i \phi_{i,1} \Big), \tag{44}$$

$$\tau \frac{\partial \phi_{i,1}}{\partial \tau} - \frac{\zeta}{2} D\phi_{i,1} + \sqrt{\tau} w D\phi_{i,0} = \delta_i (D^2 - a^{*2}) \phi_{i,1} + n_i \mathrm{Da}^* (\phi_{A,0} \phi_{B,1} + \phi_{A,1} \phi_{B,0}), \tag{45}$$

under the following boundary conditions:

$$w_1 \to 0 \quad \text{and} \quad \phi_{i,1} \to 0 \quad \text{as } \zeta \to \pm\infty. \tag{46}$$

Here, $D = \partial/\partial\zeta$, $\nabla_1^2 = -a^2$, $a^* = a\sqrt{\tau}$, $\mathrm{Da}^* = \mathrm{Da}\tau$ and a is the horizontal wave number.

For the limiting case of $\tau \to 0$, by neglecting the last term of Eq. (45), Eqs. (44) and (45) can be reduced as

$$D^2 w_1 = 0, \tag{47}$$

$$\tau \frac{\partial \phi_{i,1}}{\partial \tau} - \frac{\zeta}{2} D\phi_{i,1} + \sqrt{\tau} w_1 D\phi_{i,0} = \delta_i D^2 \phi_{i,1}. \tag{48}$$

Here $\sqrt{\tau} w_1 D\phi_{i,0}$ is kept, since $D\phi_{i,0}$ has a nonanalytic characteristic at $\tau = 0$. The solution of Eq. (47) under the boundary conditions Eqs. (46) is $w_1(\zeta) \to 0$ as $\tau \to 0$. Using this solution, the following equation can be obtained:

$$\tau \frac{\partial \phi_{i,1}}{\partial \tau} - \frac{\zeta}{2} D\phi_{i,1} = \delta_i D^2 \phi_{i,1}. \tag{49}$$

Since, the above partial differential equation is linear, by letting

$$\phi_{i,1} = \sum_{n=0}^{\infty} \varepsilon_{i,n}(\tau)\theta_{i,n}(\zeta), \tag{50}$$

one can obtain

$$\frac{1}{\varepsilon_{i,n}}\frac{d\varepsilon_{i,n}}{d\ln\tau} = \frac{1}{\theta_{i,n}}L_i\theta_{i,n} = -\lambda_n \tag{51a}$$

$$\lambda_n = \frac{n+1}{2} \quad \text{for} \quad n = 0, 1, 2, \cdots \tag{51b}$$

$$\theta_{i,n}(\zeta) = \kappa_n H_n\left(\frac{\zeta}{2\sqrt{\delta_i}}\right)\exp\left(-\frac{\zeta^2}{4\delta_i}\right), \tag{51c}$$

$$\kappa_n = \{\sqrt{(n!2^{n+1}\sqrt{\pi})}\}^{-1}, \tag{51d}$$

where $L_i = \delta_i D^2 + \frac{\zeta}{2}D$ and H_n's are the nth Hermite polynomials. Since the functions $\theta_{i,n}$'s are orthonormal, for any functions $\theta_{i,n}$ and $\theta_{i,m}$,

$$\langle\theta_{i,n}, \theta_{i,m}\rangle = \int_{-\infty}^{\infty}\theta_{i,n}\theta_{i,m}\exp\left(\frac{\zeta^2}{4\delta_i}\right)d\zeta = \delta_{nm}, \tag{52}$$

where $\exp(\zeta^2/4\delta_i)$ is the weight function of the operator L_i and δ_{nm} is the Kronecker δ.

The above results mean that the least stable disturbance is the following zeroth mode one:

$$\phi_{i,1} = \varepsilon_{i,0}(\tau)\frac{1}{\sqrt{\sqrt{\pi}}}\exp\left(-\frac{\zeta^2}{4\delta_i}\right). \tag{53}$$

Here, amplitude $\varepsilon_{i,0}(\tau)$ is governed by

$$\frac{1}{\varepsilon_{i,0}}\frac{d\varepsilon_{i,0}}{d\tau} = -\frac{1}{2\tau}. \tag{54}$$

Therefore, it may be concluded that in the early stage of diffusion the system is unconditionally stable since the least stable disturbance has a large negative growth rate. This analysis, also, can be applied to the long-wave limit $a \to 0$ and finite time, i.e., $a\sqrt{\tau} \ll 1$.

For the case of $\mathrm{Da}^* \gg 1$, the above linear stability equations can be reduced as

$$(D^2 - a^{*2})w_1^{\mathrm{T}} = -a^{*2}\left(\sum_{j,j\neq\mathrm{B}}\beta_j\phi_{j,1}\right)^{\mathrm{T}}, \tag{55a}$$

$$\tau\frac{\partial\phi_{j,1}^{\mathrm{T}}}{\partial\tau} - \frac{\zeta}{2}D\phi_{j,1}^{\mathrm{T}} + \sqrt{\tau}w_1^{\mathrm{T}}D\phi_{j,0}^{\mathrm{T}} = \delta_j(D^2 - a^{*2})\phi_{j,1}^{\mathrm{T}}, \tag{56a}$$

for the top layer ($-\infty < \zeta < \zeta_f$), and

$$(D^2 - a^{*2})w_1^{\mathrm{B}} = -a^{*2}\left(\sum_{k,k\neq\mathrm{A}}\beta_k\phi_{k,1}\right)^{\mathrm{B}}, \tag{55b}$$

$$\tau\frac{\partial\phi_{k,1}^{\mathrm{B}}}{\partial\tau} - \frac{\zeta}{2}D\phi_{k,1}^{\mathrm{B}} + \sqrt{\tau}w_1^{\mathrm{B}}D\phi_{k,0}^{\mathrm{B}} = \delta_k(D^2 - a^{*2})\phi_{k,1}^{\mathrm{B}}, \tag{56b}$$

for the bottom layer ($\zeta_f < \zeta < \infty$), where $D = \partial/\partial\zeta$. The matching and boundary conditions are

$$w_1^{\mathrm{T}} = w_1^{\mathrm{B}} \quad \text{and} \quad Dw_1^{\mathrm{T}} = Dw_1^{\mathrm{B}} \quad \text{at } \zeta = \zeta_f, \tag{57a}$$

$$\left(\sum_{j,j\neq \mathrm{B}} \phi_{j,1}\right)^{\mathrm{T}} = \left(\sum_{j,j\neq \mathrm{B}} \phi_{j,1}\right)^{\mathrm{B}} \quad \text{and} \quad \left(\sum_{k,k\neq \mathrm{A}} \phi_{k,1}\right)^{\mathrm{T}} = \left(\sum_{k,k\neq \mathrm{A}} \phi_{k,1}\right)^{\mathrm{B}} \quad \text{at } \zeta = \zeta_f, \tag{57b}$$

$$\left(\sum_{j,j\neq \mathrm{B}} \delta_j D\phi_{j,1}\right)^{\mathrm{T}} = \left(\sum_{j,j\neq \mathrm{B}} \delta_j D\phi_{j,1}\right)^{\mathrm{B}} \quad \text{and}$$

$$\left(\sum_{k,k\neq \mathrm{A}} \delta_k D\phi_{k,1}\right)^{\mathrm{T}} = \left(\sum_{k,k\neq \mathrm{A}} \delta_k D\phi_{k,1}\right)^{\mathrm{B}} \quad \text{at } \zeta = \zeta_f, \tag{57c}$$

$$w_1 \to 0 \quad \text{and} \quad \phi_{i,1} \to 0 \quad \text{as } \zeta \to \pm\infty. \tag{57d}$$

Because the two reactants A and B cannot coexist for the infinitely fast reaction system, Eqs. (57b) and (57c) means that the concentrations of (A+C) and (B+C), and their fluxes should be continuous. So, it is natural that $\phi_{\mathrm{B},1}^{\mathrm{T}} = 0$ and $D\phi_{\mathrm{B},1}^{\mathrm{T}} = 0$ for $\zeta \leqslant \zeta_f$, $\phi_{\mathrm{A},1}^{\mathrm{B}} = 0$ and $D\phi_{\mathrm{A},1}^{\mathrm{B}} = 0$ for $\zeta \geqslant \zeta_f$. From these relations, the above matching conditions Eqs. (54b) and (54c) can be reduced as

$$\phi_{\mathrm{A},1}^{\mathrm{T}} = -\phi_{\mathrm{B},1}^{\mathrm{B}}, \quad \phi_{\mathrm{C},1}^{\mathrm{T}} = \phi_{\mathrm{B},1}^{\mathrm{B}} + \phi_{\mathrm{C},1}^{\mathrm{B}}, \quad D\phi_{\mathrm{A},1}^{\mathrm{T}} = -\delta_{\mathrm{B}} D\phi_{\mathrm{B},1}^{\mathrm{B}}, \quad \text{and}$$
$$D\phi_{\mathrm{C},1}^{\mathrm{T}} = D\phi_{\mathrm{C},1}^{\mathrm{B}} + \delta_{\mathrm{C}}^{-1}\delta_{\mathrm{B}} D\phi_{\mathrm{B},1}^{\mathrm{B}} \quad \text{at } \zeta = \zeta_f \tag{58}$$

Here, we should stress that the continuities of the product C and its flux are not imposed at $\zeta = \zeta_f$.

B. Solution methods

For the limiting case of $\delta_{\mathrm{B}} = \delta_{\mathrm{C}} = 1$, Kim [16] solved the above stability Eqs. (55)–(57) analytically. However, since his analytic approach cannot be applied to the present different diffusivities case, we should introduce the following quasi-steady state approximation in the (τ, ζ)-domain, here we refer the present QSSA as QSSAζ:

$$[w_1(\tau, \zeta), \phi_{i,1}(\tau, \zeta)] = [w_1(\zeta), \phi_{i,1}(\zeta)] \exp(\sigma^* \tau), \tag{59}$$

and we solve the resulting stability equation numerically. In the present study, we have tried to solve the stability Eqs. (52)–(55) with the numerical shooting method [27].

For the limiting case of $\delta_{\mathrm{B}} = \delta_{\mathrm{C}} = 1$, the neutral stability curves, which correspond to $\sigma^* = 0$, obtained from the analytical approximation without the QSSA and the present numerical shooting solution with QSSA, are compared in Fig. 2. As shown in this Fig. 2, the present numerical solution and the previous analytical approximations are in good agreement. In other words, the present QSSAζ is robust, and the numerical solution method is accurate.

V. NUMERICAL SIMULATIONS

Even though the above asymptotic and linear analyses give useful information on the onset and the growth of the instabilities, a more exact solution can be obtained by solving the initial value problem of Eqs. (6)–(8). For the infinite Da case, by assuming that both reactants cannot coexist, Eqs. (7)–(9) can be rewritten as

$$\nabla^2 \psi = -\omega_y, \tag{60}$$

$$\frac{\partial \phi_{i,1}}{\partial \tau} + j_i = \delta_i \nabla^2 \phi_{i,1}, \tag{61}$$

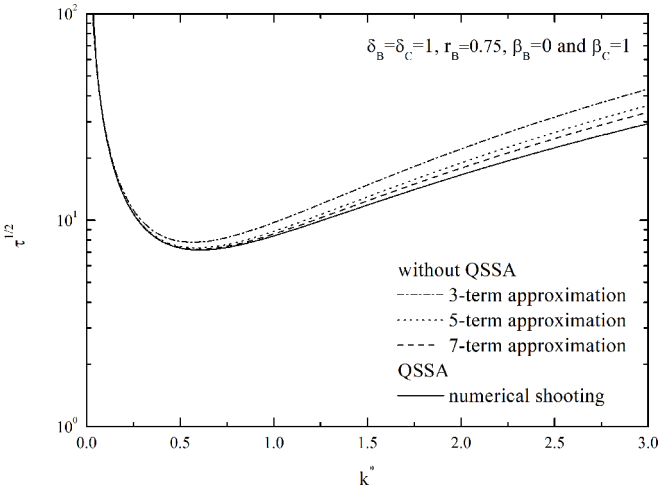

FIG. 2. Comparison of neutral stability curves obtained from analytic approximation without the QSSA and the present numerical shooting method with the QSSA for the limiting case of $\delta_B = \delta_C = 1$.

$$\omega_y = -\sum_i \beta_i \frac{\partial \phi_{i,1}}{\partial x}, \tag{62}$$

$$j_i = \left(\frac{\partial \psi}{\partial x}\frac{\partial \phi_{i,0}}{\partial z} + \frac{\partial \psi}{\partial x}\frac{\partial \phi_{i,1}}{\partial z} - \frac{\partial \psi}{\partial z}\frac{\partial \phi_{i,1}}{\partial x} \right), \tag{63}$$

under the following boundary conditions:

$$\psi \to 0 \quad \text{and} \quad \phi_{i,1} \to 0 \quad \text{as } z \to \pm\infty. \tag{64}$$

Here, using the stream function ψ, we expressed the two-dimensional velocity filed as $(u, w) = (-\partial\psi/\partial z, \partial\psi/\partial x)$. To solve Eqs. (60)–(64) accurately, we have employed the Fourier-spectral numerical scheme described in Tan and Homsy [28]. The periodic boundary conditions are taken in both the x and z direction. The use of these boundary conditions has no influence on the dynamics of the chemical front as long as the unstable propagating front does not encounter its periodic extension. In the present study, the calculation domain is set as $[0, 2 \times 10^3] \times [-10^3, 10^3]$, and 2048×2048 collocation points are used. Unlike the linear theory, the initiation condition is important in the nonlinear analysis. Since, the initial growth rate analysis cannot suggest the dominant wavenumber, in the present study, the following initial condition is employed:

$$\phi_{i,1} = \varepsilon_{i,0}(\tau)\frac{1}{\sqrt{\sqrt{\pi}}} \exp\left(-\frac{\zeta^2}{4\delta_i}\right) \text{rand}(x) \quad \text{at } \tau = \tau_i, \tag{65}$$

where ε means the initial disturbance level and rand(x) is the pseudorandom number uniformly distributed between -1 and 1. This condition prevents unphysical conditions of $\phi_i > 1$ or $\phi_i < 0$, if ε is small enough. From Eq. (53), it can be easily understood that the above initial condition corresponds to the least stable zeroth mode of disturbance. In the present study, we set $\varepsilon = 10^{-2}$. For region of $\tau \sim 0$, the base concentration gradient $\frac{\partial \phi_{i,0}}{\partial z}(\sim\delta(z))$ shows the nonanalytic feature and leads to bad convergence properties. For this reason, at all the nonlinear numerical simulations, the disturbance given in Eq. (65) is introduced at $\tau_i = 0.1$.

Here, since we are interested in the enhancement of mixing or mass transfer driven by the instability motion, let us consider the mass transfer rate of (A + C). The dimensionless mass flux J at the reaction front $z = z_f$, which can be written as the sum of contributions from the base diffusion

state, J_0, and the convective motion, J_1:

$$J = J_0 + J_1. \tag{66}$$

The diffusional flux can be computed explicitly from the base concentration profile as

$$J_0 = -\left(\frac{\partial \phi_{\mathrm{A},0}}{\partial z} + \delta_{\mathrm{C}} \frac{\partial \phi_{\mathrm{C},0}}{\partial z}\right)\bigg|_{z=z_f} = \frac{1}{\sqrt{\pi \tau}} \left\{ \frac{\exp\left(-\zeta_f^2/4\right)}{\mathrm{erfc}(-\zeta_f/2)} - r_{\mathrm{C}} \sqrt{\delta_{\mathrm{C}}} \frac{\exp\left(-\zeta_f^2/4\delta_{\mathrm{C}}\right)}{\mathrm{erfc}(-\zeta_f/\sqrt{4\delta_{\mathrm{C}}})} \right\}. \tag{67}$$

The flux from convective motion are obtained as [29]

$$J_1 = \frac{1}{L_x} \int_0^{L_x} \left(-\frac{\partial \phi_{\mathrm{A},1}}{\partial z} - \delta_{\mathrm{C}} \frac{\partial \phi_{\mathrm{C},1}}{\partial z}\bigg|_{z=z_f} \right) dx = \frac{1}{L_x} \frac{1}{L_z} \int_0^{L_x} \int_{-L_z/2}^{L_z/2} w(\phi_{\mathrm{A},1} + \phi_{\mathrm{C},1}) dz dx. \tag{68}$$

We defined another important quantity, the intensity of the vorticity as

$$|\omega_y| = \left[\int_0^{L_x} \int_{-L_z/2}^{L_z/2} \omega_y^2 dz dx \right]^{1/2}. \tag{69}$$

For the limiting case of $\delta_{\mathrm{B}} = \delta_{\mathrm{C}} = 1$, $r_{\mathrm{B}} = 0.75$, $\beta_{\mathrm{B}} = 0$, and $\beta_{\mathrm{C}} = 1$, the temporal evolutions of total flux and the intensity of the vorticity are given in Fig. 3. As shown in this figure, the time from which the vorticity field starts to grow is nearly the same as the critical time determined from the present linear stability analysis (see Fig. 2). In addition, the vorticity field becomes visible from the time at which the total flux shows its minimum.

VI. RESULTS AND DISCUSSION

For the nonreactive system, i.e., $\mathrm{Da} = 0$, Trevelyan *et al.* [15] conducted linear and nonlinear analyses and concluded that the system is unconditionally stable if

$$1 < \delta_{\mathrm{B}} < (\beta_{\mathrm{B}} r_{\mathrm{B}})^{2/3}. \tag{70}$$

Recently, Kim and Song [22] drew the same result by employing the following conditions:

$$\frac{d\bar{\rho}_0}{d\zeta}\bigg|_{\zeta=0} > 0, \quad \zeta_e^2 < 0 \quad \text{and} \quad \zeta_i^2 < 0. \tag{71}$$

The above conditions mean that the fluid layer is gravitationally stable if the density of the system increases according to the gravity field without its inflection points. In Trevelyan *et al.*'s [15] linear stability analysis, they employed the QSSA in the (τ, z)-domain or frozen-time; here we refer to the conventional QSSA as QSSAz. Under this QSSAz, the disturbance quantities are expressed as

$$[w_1(\tau, z), \phi_{i,1}(\tau, z)] = [w_1(z), \phi_{i,1}(z)] \exp(\sigma \tau). \tag{72}$$

By applying the above QSSAz into Eqs. (41) and (42), the following stability equations can be obtained:

$$\left(\frac{d^2}{dz^2} - a^2\right) w_1 = -a^2 \left(\sum\nolimits_i \beta_i \phi_{i,1} \right), \tag{73}$$

$$\sigma \phi_{i,1} + w_1 \frac{\partial \phi_{i,0}}{\partial z} = \delta_i \left(\frac{d^2}{dz^2} - a^2\right) \phi_{i,1} + n_i \mathrm{Da}(\phi_{\mathrm{A},0} \phi_{\mathrm{B},1} + \phi_{\mathrm{A},1} \phi_{\mathrm{B},0}). \tag{74}$$

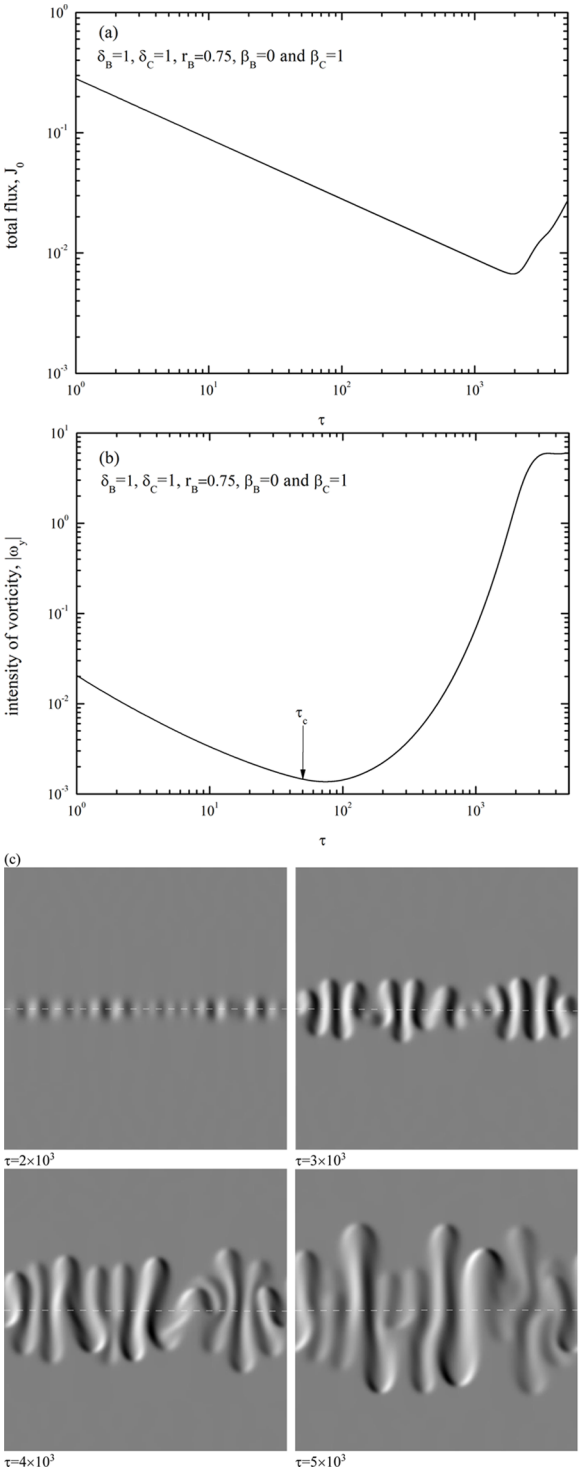

FIG. 3. Temporal evolution of (a) total flux, (b) intensity of vorticity, and (c) vorticity field for the limiting case of $\delta_B = \delta_C = 1$, $r_B = 0.75$, $\beta_B = 0$, and $\beta_C = 1$. Here, τ_c is obtained from the linear stability analysis.

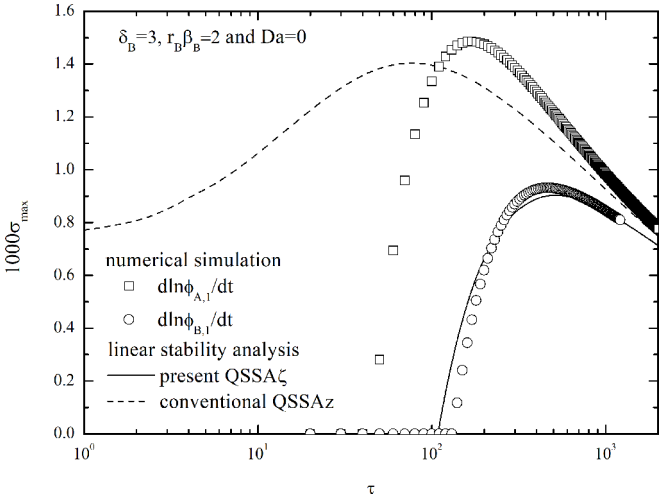

FIG. 4. Comparison between the present QSSAζ and the conventional QSSAz (Trevelyan *et al.* [15]) for the nonreactive case, i.e., Da = 0. The previous numerical simulations (Trevelyan *et al.* [15]) are also compared.

For the nonreactive case, i.e., Da = 0, Trevelyan *et al.* [15] solved the above stability equation. They suggested that based on the QSSAz, the initial growth rate becomes

$$1-\frac{a}{\sqrt{a^2+\sigma}}=r_{\mathrm{B}}\beta_{\mathrm{B}}\left(1-\frac{a}{\sqrt{a^2+(\sigma/\delta_{\mathrm{B}})}}\right)+\frac{2\sigma}{a}\quad\text{for Da}=0\quad\text{and}\quad\tau=0. \tag{75}$$

Furthermore, at the limiting case of $\tau = 0$, the above relation can be used for the nonzero Da system because both reactants cannot coexist with $\phi_{\mathrm{C}} = 0$ at $\tau = 0$. However, the present initial growth rate analysis without QSSA summarized in Eq. (54) yields

$$\sigma^* \to -\frac{1}{2\tau}\quad\text{as}\ \tau\to 0. \tag{76}$$

For the example case of Da = 0, $\delta_{\mathrm{B}} = 3$, and $r_{\mathrm{B}}\beta_{\mathrm{B}} = 2$, Eq. (75) yields

$$\sigma_{\max}=7.4364\times10^{-4}\quad\text{and}\quad a_{\max}=0.05045\quad\text{for}\ \tau=0. \tag{77}$$

The above relation means that this example system is initially unstable. However, the present Eq. (76) proposed that the initial growth rate is a large negative. For this example case, the present QSSAζ in the (τ, ζ)-domain is compared with Trevelyan *et al.*'s [15] QSSAz and numerical simulations in Fig. 4. As shown in Fig. 4, it is clear that Eqs. (75) and (76) suggest the limiting cases of the QSSAz and QSSAζ, respectively. Furthermore, Fig. 4 shows that the present QSSAζ explains Trevelyan *et al.*'s [15] numerical simulation more reasonably than Trevelyan *et al.*'s [15] conventional QSSAz especially for the small time region.

For the limiting case of $\delta_{\mathrm{B}} = \delta_{\mathrm{C}} = 1$, in the (τ, ζ)-domain, the linear stability analysis without the QSSA was conducted for the reactive system [13]. As discussed in Fig. 2, in the (τ, ζ)-domain, the stability characteristics obtained from analytic approximations without QSSA and the numerical solution under the QSSAζ are consistent. However, the QSSAz in the (τ, z)-domain has not been supported by the linear stability analysis without QSSA. Therefore, for the small-time region, the linear stability analyses in the (τ, ζ)-domain are strongly recommended, and therefore we used QSSAζ in the present linear analysis.

Because, as discussed by Trevelyan *et al.* [17], a total of 62 density profiles are possible, we will conduct linear and nonlinear analyses for some typical cases. At first, we considered

the possibility of the gravitational instability without an adverse density gradient. In case of the stationary reaction front, i.e., $\zeta_f = 0$, the effect of the bottom layer density profile on the onset and the growth of instabilities are summarized in Fig. 5. For the case of $\beta_B < U_2 L_2^{-1} \delta_C$, i.e., the RT regime, the large density difference accelerates the onset of instabilities [see Figs. 5(a) and 5(b)] and the growth of convective motion [see Figs. 5(a), 5(c), and 5(d)]. In addition, for the case of $U_2 L_2^{-1} \delta_C < \beta_B < U_2 L_2^{-1} \delta_B$, i.e., the DD regime, the onset and the growth of gravitational instability is possible without density inversion. Furthermore, for the stability limit, $\beta_B = U_2 L_2^{-1} \delta_B$, we cannot expect the onset of instability [see Fig. 5(b)] and the growth of the convective motion [see Fig. 5(d)]. The present findings suggest that the unconditionally stable conditions suggested by Eq. (38) and the present linear stability analysis [see Fig. 5(b)] and the numerical simulation [see Fig. 5(c)] are in good agreement. Even though the neutrally stable region of the top layer retards the growth of the convective motion, it cannot prevent the convective motion from developing in the top layer [see Fig. 5(d)].

For the neutrally stable bottom layer, the density profile of the top layer and its effect on the critical time is given in Figs. 6(a) and 6(b). These figures also show that in multicomponent systems, the onset of gravitational instabilities are possible without density inversion, i.e., in the DD regime ($U_2 < \beta_C < \delta_C U_2$). For this case, Trevelyan *et al.*'s [17] general classification, Eq. (39), and the present asymptotic stability criterion are identical since $L_1 = L_2$ if $\zeta_f = 0$, and the present asymptotic stability analysis explains the present linear stability analysis quite well. As discussed in the above, we cannot expect the onset and the growth of instabilities for the stability limit, i.e., $\beta_C = \delta_C U_2$ [see Figs. 6(b) and 6(c)]. In addition, unlike the system considered in Fig. 5, the strong stability barrier of the bottom layer prevents the convective motion from developing in the bottom layer [see Fig. 6(d)].

For the case of $\zeta_f < 0$, i.e., the reaction front moves upward, the top layer is neutrally stable if $\beta_C = \delta_C U_2$ and $\delta_C > 1$ [see Eq. (29)]. For this case, the effect of β_B on the density profile, critical time, and the temporal growth of the vorticity field are summarized in Figs. 7(a)–7(c). As shown in Fig. 7(b), the system can be unstable even for the Trevelyan *et al.*'s [17] unconditionally stable regime ($U_2 L_2^{-1} \delta_B < \beta_B < U_2 L_1^{-1} \delta_B$). However, as shown in Fig. 7(c), we cannot confirm the validity of the present linear analysis because the critical time from which the intensity of the vorticity starts to grow is too large to trace it by the present numerical simulation. Comparing Figs. 5(d) and 7(d), we cannot find any critical effect of the location of the reaction front, ζ_f on the development of the convective motion.

We also conducted a similar work for the case of $\zeta_f > 0$, i.e., the reaction front moves downward. As shown in Figs. 8(b) and 8(c), the difference between the present work and the previous Trevelyan *et al.*'s [17] general classification is not critical, because for the present case, the values of L_1 and L_2 are nearly the same. Comparing Figs. 5(d), 7(d), and 8(d), we cannot find any critical effect of ζ_f except for the movement of the reaction front.

For the HCl+MOH→NaCl system, where M = Li, Na, K, and Cs, Almarcha *et al.* [9,10] conducted experiments and numerical simulations to study the effect of a chemical acid-base reaction on the growth of gravitational instabilities. According to their results, the convective motions are strongly affected by the density profiles. As discussed by Trevelyan *et al.* [17], in some special cases, the density profiles show a very interesting feature. For two exemplary cases, the concentration and density profiles, corresponding neutral stability curves and the vertical velocity component profiles are given in Figs. 9 and 10. The density profile given in Figs. 9(a) suggests there exist two separate unstable regions and the density difference of the top layer is larger than that of the bottom one. According to the present linear stability analysis, the top layer is much more unstable than the bottom layer and the instability cannot be expected for $\tau < 10^4$. As shown in Fig. 9(b), the present QSSAζ predicts the existence of the forbidden region where instabilities are not possible, however, the conventional QSSAz does not. This is the critical difference between the present QSSAζ and the conventional QSSAz. The normalized vertical velocity disturbances at the minima of the two neutral stability curves are given in Fig. 9(c). As expected from the density profile

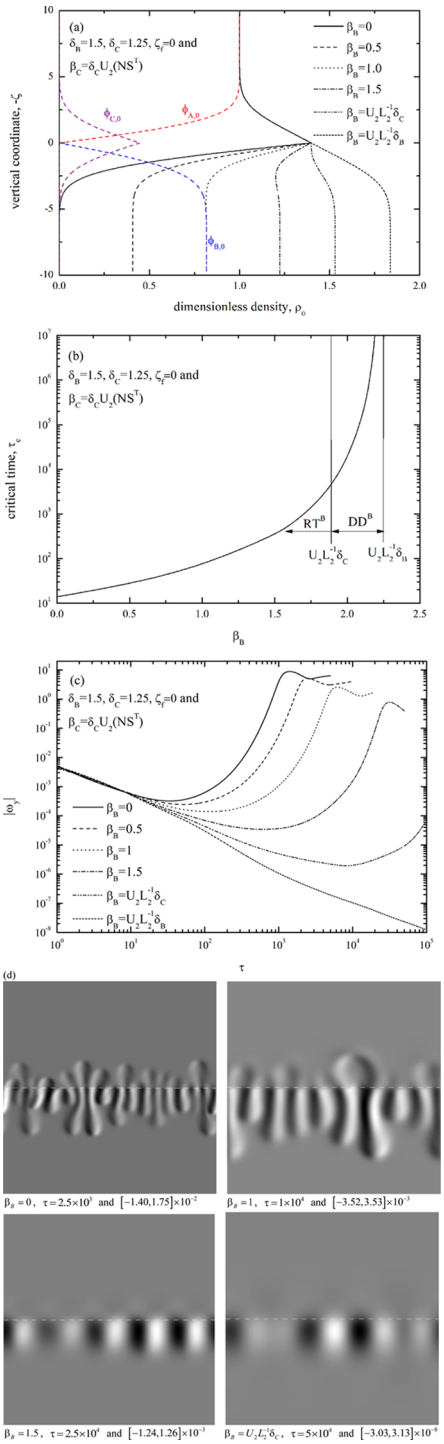

FIG. 5. Effect of β_B on the (a) density profile, (b) critical time, (c) temporal evolution of the intensity of vorticity, and (d) vorticity field, where numbers in the brackets correspond to $[\omega_{y,\min}, \omega_{y,\max}]$, for the case of $\zeta_f = 0$ and neutrally stable top layer.

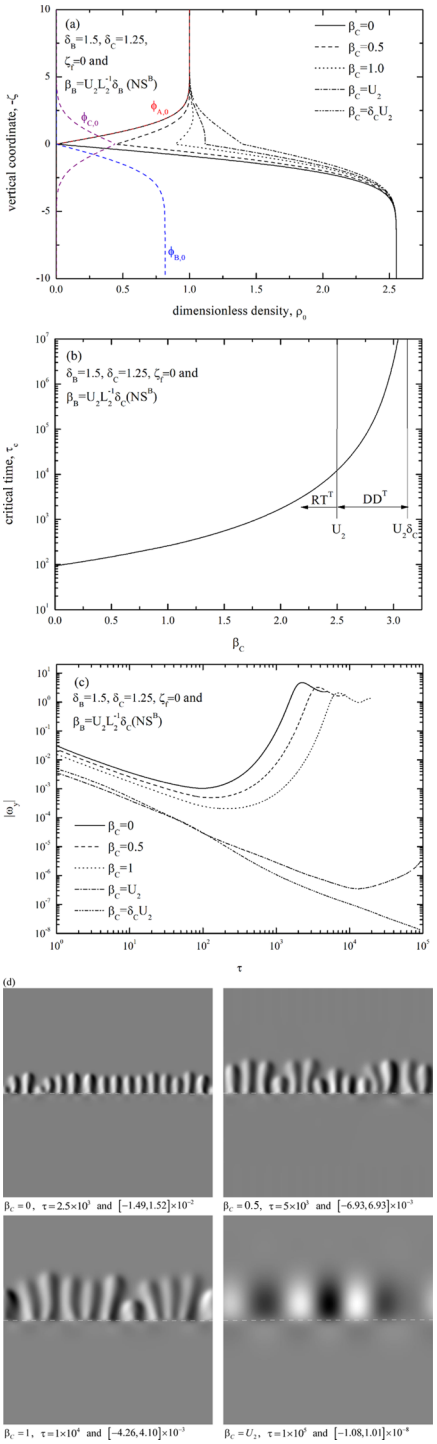

FIG. 6. Effect of β_C on the (a) density profile, (b) critical time, (c) temporal evolution of intensity of vorticity and (d) vorticity field, where numbers in the brackets correspond to $[\omega_{y,\min}, \omega_{y,\max}]$, for the case of $\zeta_f = 0$ and neutrally stable bottom layer.

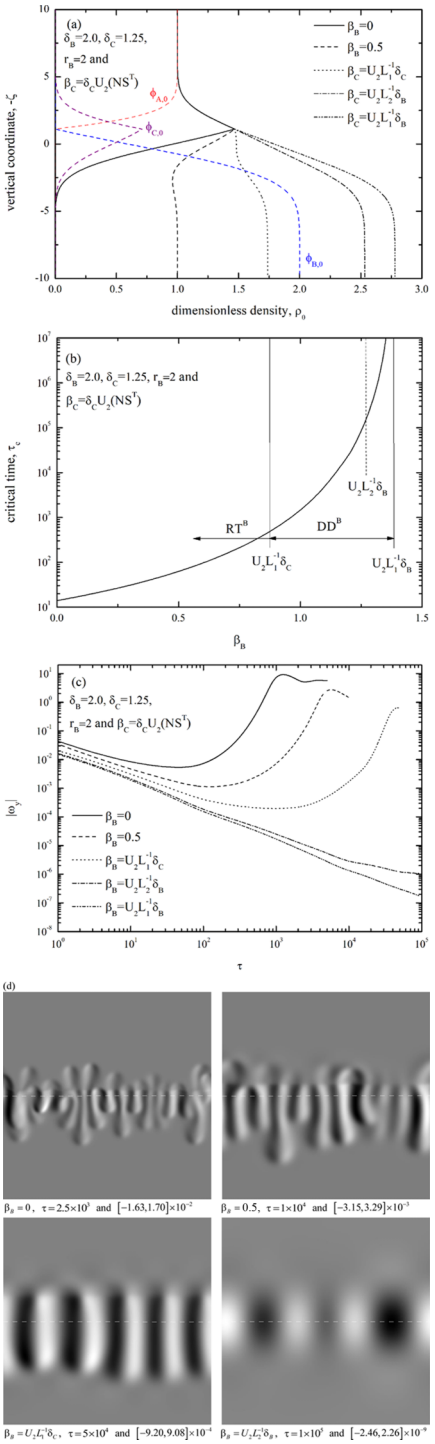

FIG. 7. Effect of β_B on the (a) density profile and (b) critical time, (c) temporal evolution of the intensity of the vorticity, and (d) vorticity field, where numbers in the brackets correspond to $[\omega_{y,\min}, \omega_{y,\max}]$, for the case of $\zeta_f < 0$, the reaction front moving upward.

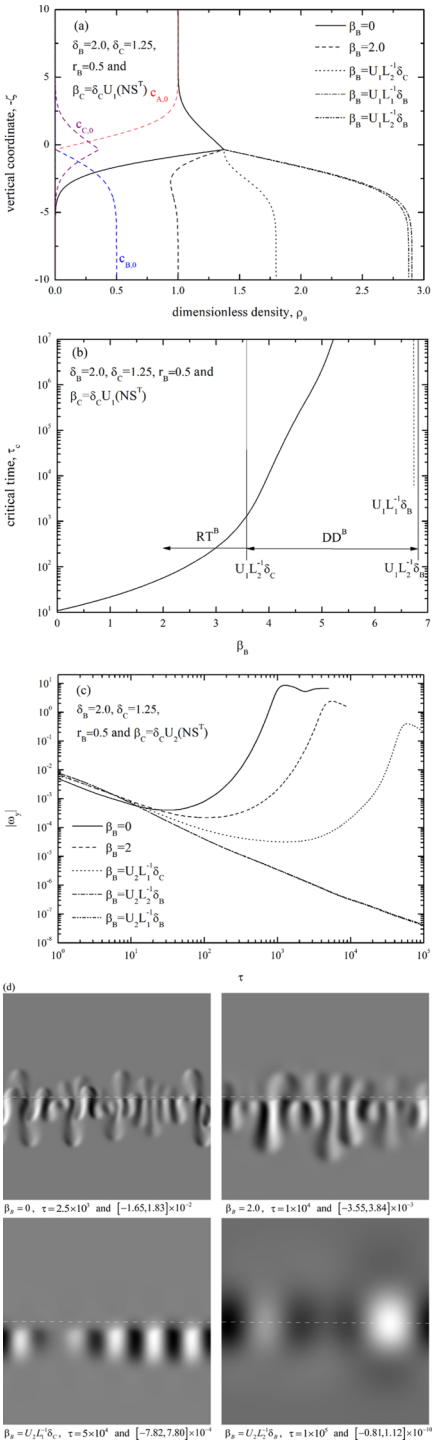

FIG. 8. Effect of β_{B} on the (a) density profile and (b) critical time, (c) temporal evolution of the intensity of the vorticity, and (d) vorticity field, where numbers in the brackets correspond to $[\omega_{y,\min}, \omega_{y,\max}]$, for the case of $\zeta_f > 0$, the reaction front moving downward.

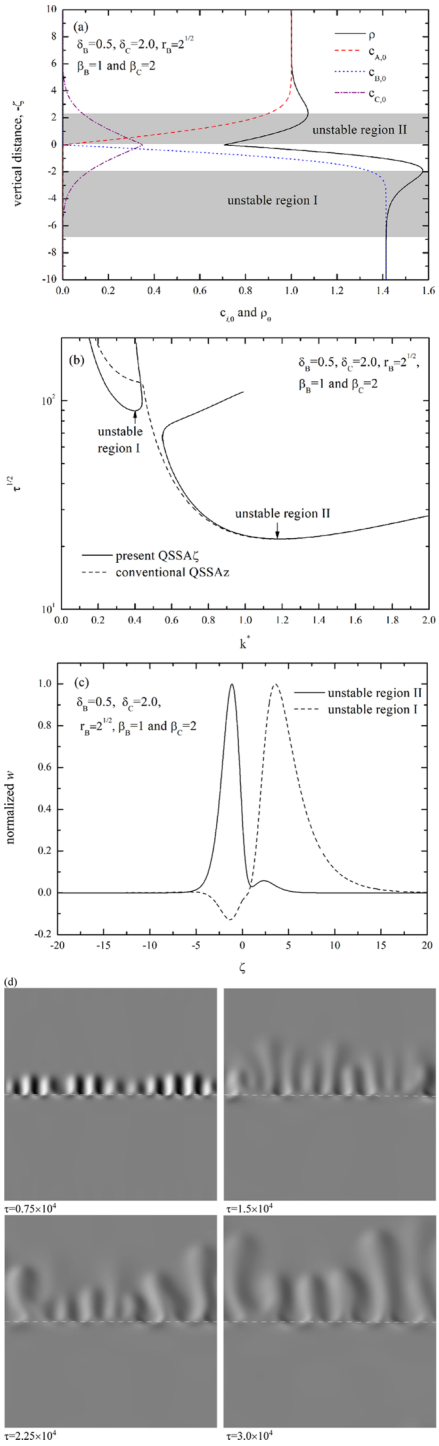

FIG. 9. Stability characteristics for the case of $\delta_B = 0.5$, $\delta_C = 2.0$, $r_B = \sqrt{2}$, $\beta_B = 1$, and $\beta_C = 2$. (a) Concentration and density profiles, (b) neutral stability curves, (c) normalized vertical velocity disturbance and (d) temporal evolution of vorticity field where $[\omega_{y,\min}, \omega_{y,\max}] = [-5.2, 5.2] \times 10^{-3}$.

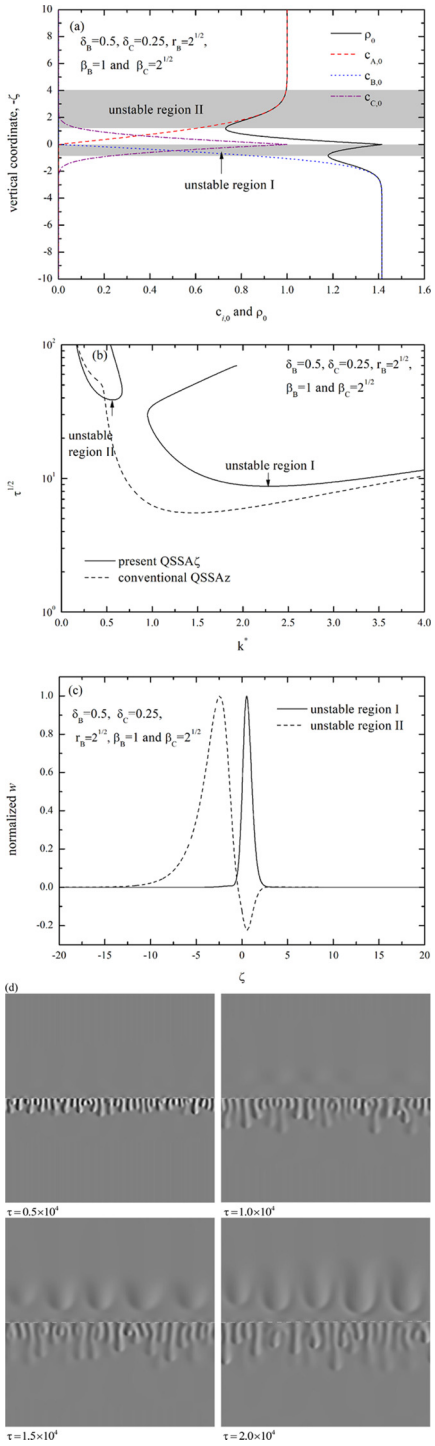

FIG. 10. Stability characteristics for the case of $\delta_B = 0.5$, $\delta_C = 0.25$, $r_B = 2^{1/2}$, $\beta_B = 1$, and $\beta_C = 2^{1/2}$. (a) Concentration and density profiles, (b) neutral stability curves, (c) normalized vertical velocity disturbance, and (d) temporal evolution of vorticity field where $[\omega_{y,\min}, \omega_{y,\max}] = [-0.01, 0.01]$.

of Fig. 9(a), the instability of the top layer (negative ζ region) is confined within a narrower region than the instability of the bottom layer. The results of the present linear analysis were validated by the nonlinear numerical simulations. The temporal evolution of the vorticity field for the system of Fig. 9(a) is summarized in Fig. 9(d). The bottom layer instabilities are not visible until $\tau < 3 \times 10^4$

As far as we know, the physical reality of the density profile given in Fig. 9(a) is not reported. However, the density profile given in Fig. 10(a) is quite similar to that of Bratsun *et al.*'s [30] concentration dependent convection (CDC) system (see Fig. 3(a) of Bratsun *et al.* [30]). Even though the present neutral stability curves are quite different from Bratsun *et al.*'s (see Fig. 3(b) of Bratsun *et al.* [30]), Figs. 10(b) and 10(c), and Bratsun *et al.*'s [30] experiments and numerical simulation show that initially the instabilities are confined within the narrow region just below the reaction front, and then the top layer instabilities become visible as time goes on. This means that the present linear and nonlinear analyses are in good agreement with the previous experimental and numerical work.

VII. CONCLUSIONS

For the infinitely fast reaction system, the effect of different diffusivities of reactants and product on the onset and growth of the gravitational instability in a Hele-Shaw cell was analyzed using an asymptotic and a linear stability theory and the nonlinear direct numerical simulation. Without a systematic stability analysis, the asymptotic stability criteria were proposed and suggested that the instabilities are possible without the adverse density gradients. Also, we compared the present asymptotic stability criteria with the systematic linear stability analysis and nonlinear numerical simulations. For some interesting cases, we performed the linear stability analyses and the nonlinear numerical simulations and showed that two separate modes of instabilities are possible even for the constant diffusivities system. Based on the present study, the present asymptotic, linear, and nonlinear analyses can be used to study the stability of multicomponent systems.

ACKNOWLEDGMENT

This research was supported by the Basic Science Research Program through the National Research Foundation of Korea (NRF) funded by the Ministry of Education (KR) (Grant No. NRF-2018R1D1A3A03000703).

[1] L. Rayleigh, Investigation of the character of the equilibrium of an incompressible heavy fluid of variable density, Proc. London Math. Soc. **s1-14**, 170 (1882).

[2] G. I. Taylor, The instability of liquid surfaces when accelerated in a direction perpendicular to their planes, Proc. R. Soc. London Ser. A **201**, 192 (1950).

[3] R. A. Wooding, The stability of an interface between miscible fluids in a porous medium, ZAMP **13**, 255 (1962).

[4] G. Bazsa and I. R. Epstein, Traveling waves in the nitric acid-iron(II) reaction, J. Phys. Chem. **89**, 3050 (1985).

[5] I. Nagypál, G. Bazsa, and I. R. Epstein, Gravity-induced anisotropies in chemical waves, J. Am. Chem. Soc. **108**, 3635 (1986).

[6] O. Citri, M. L. Kagan, R. Kosloff, and D. Avnir, Evolution of chemically induced unstable density gradient near horizontal reactive interface, Langmuir **6**, 559 (1990).

[7] A. J. Pons, F. Sagués, M. A. Bees, and P. G. Sørensen, Pattern formation in the methylene-blue system, J. Phys. Chem. B **104**, 2251 (2000).

[8] C. Wylock, S. Dehaeck, A. Rednikov, and P. Coliner, Chemo-hydrodynamical instability created by CO_2 absorption in an aqueous solution of $NaHCO_3$ and Na_2CO_3, Microgravity Sci. Technol. **20**, 171 (2008).

[9] C. Almarcha, P. M. J. Trevelyan, P. Grosfils, and A. de Wit, Chemically Driven Hydrodynamic Instabilities, Phys. Rev. Lett. **104**, 044501 (2010).
[10] C. Almarcha, Y. R'Honi, Y. De Decker, P. M. J. Trevelyan, K. Eckert, and A. de Wit, Convective mixing induced by acid-base reactions, J. Phys. Chem. B **115**, 9739 (2011).
[11] S. Kuster, L. A. Riolfo, A. Zalts, C. El Hasi, C. Almarcha, P. M. J. Trevelyan, A. de Wit, and A. D'Onofrio, Differential diffusion effects on buoyancy-driven instabilities of acid-base fronts: The effect of color indicator, Phys. Chem. Chem. Phys. **13**, 17295 (2011).
[12] L. Lemaigre, M. A. Budroni, L. A. Riolfo, and P. Grosfils, Asymmetric Rayleigh-Taylor and double-diffusive fingers in reactive systems, Phys. Fluids **25**, 014103 (2013).
[13] S. H. Hejazi and J. Azaiez, Stability of reactive interface in saturated porous media under gravity in the presence of transverse flows, J. Fluid Mech. **695**, 439 (2012).
[14] S. H. Hejazi and J. Azaiez, Nonlinear simulation of transverse flow interactions with chemically driven convective mixing in porous media, Water Res. Res. **49**, 4607 (2013).
[15] P. M. J. Trevelyan, C. Almarcha, and A. de Wit, Buoyancy-driven instabilities of miscible two-layer stratifications in porous media and Hele-Shaw cells, J. Fluid Mech. **670**, 38 (2011).
[16] M. C. Kim, Effect of irreversible A+B→C reaction on the onset and the growth of the buoyancy-driven instability in a porous medium, Chem. Eng. Sci. **112**, 56 (2014).
[17] P. M. J. Trevelyan, C. Almarcha, and A. De Wit, Buoyancy-driven instabilities around miscible A+B→C reaction fronts: A general classification, Phys. Rev. E **91**, 023001 (2015).
[18] L. Rongy, P. M. J. Trevelyan, and A. De Wit, Dynamics of A+B→C Reaction Fronts in the Presence of Buoyancy-Driven Convection, Phys. Rev. Lett. **101**, 084503 (2008).
[19] H. E. Huppert and P. C. Manins, Limiting conditions for salt-fingering at an interface, Deep-Sea Res Oceanographic Abstracts. **20**, 315 (1973).
[20] L. Costantino, C. D. Volpe, O. Ortona, and C. Vitagliano, Isothermal diffusion in a peculiar ternary system: The microemulsion AOT-water-heptane, J. Chem. Soc. Faraday Trans. **88**, 61 (1992).
[21] P. Vitagliano, L. Ambrosone, and V. Vitagliano, Gravitational instabilities in multicomponent free-diffusion boundaries, J. Phys. Chem. **96**, 1431 (1992).
[22] M. C. Kim and K. H. Song, Effect of cross-diffusion on the gravitational instability in a ternary mixture: Asymptotic and linear analyses, Chem. Eng. Sci. **191**, 191 (2018).
[23] M. C. Kim and S. S. S. Cardoso, Diffusivity ratio effect on the onset of the buoyancy-driven instability of an A+B→C chemical reaction system in a Hele-Shaw cell: Asymptotic and linear stability analyses, Phys. Fluids **30**, 094102 (2018).
[24] Y. Ben, E. A. Demekhin, and H.-C. Chang, A spectral theory for small-amplitude miscible fingering, Phys. Fluids **14**, 999 (2002).
[25] D. Pritchard, The linear stability of double-diffusive miscible rectilinear displacements in a Hele-Shaw cell, Eur. J. Mech. (B/Fluids) **28**, 564 (2009).
[26] A. Riaz, M. Hesse, H. A. Tchelepi, and F. M. Orr Jr., Onset of convection in a gravitationally unstable diffusive boundary layer in porous media, J. Fluid Mech. **548**, 87 (2006).
[27] M. C. Kim, Energy stability analysis on the onset of buoyancy-driven convection in a horizontal fluid layer subject to evaporative cooling, Korean Chem. Eng. Res. **57**, 142 (2019).
[28] C. T. Tan and G. M. Homsy, Simulation of nonlinear viscous fingering in miscible displacement, Phys. Fluids **31**, 1330 (1988).
[29] J. T. H. Andres and S. S. S. Cardoso, Convection and reaction in a diffusive boundary layer in a porous medium: Nonlinear dynamics, Chaos **22**, 037113 (2012).
[30] D. Bratsun, K. Kostarev, A. Mizev, and E. Mosheva, Concentration-dependent diffusion instability in reactive miscible fluids, Phys. Rev. E **92**, 011003(R) (2015).